We are IntechOpen, the world's leading publisher of Open Access books
Built by scientists, for scientists

6,500
Open access books available

176,000
International authors and editors

190M
Downloads

Our authors are among the

154
Countries delivered to

TOP 1%
most cited scientists

12.2%
Contributors from top 500 universities

WEB OF SCIENCE™

Selection of our books indexed in the Book Citation Index
in Web of Science™ Core Collection (BKCI)

Interested in publishing with us?
Contact book.department@intechopen.com

Numbers displayed above are based on latest data collected.
For more information visit www.intechopen.com

Chapter

Holographic Beamforming

Ali Araghi and Mohsen Khalily

Abstract

This chapter presents the fundamentals of the holography technique to form the beam in electromagnetic (EM) structures. The application of holography in leaky-wave antennas, metasurface reflectors, and reconfigurable intelligent surfaces (RISs) is explained. Consequently, different methods to analyze and realize an EM hologram are presented. A comparison is made between forming the beam via holographic-based radiators, phased-array antennas, and MIMO systems. The thing which is common between these three is that all of them can contain a number of elements that are repeated in a fashion. However, the functionality of these elements in the three mentioned structures is totally different from each other. This concept is explained in detail in this chapter.

Keywords: holography technique, leaky-wave antenna, metasurface, periodic structures, MIMO systems, phased-array antenna

1. Introduction

Consider a case where an electromagnetic (EM) aperture with an arbitrary geometry is placed on the xy plane as shown in **Figure 1(a)**. To have the ability to form the constructed beam, it is required to control both phase constant (β) and amplitude (α) of the EM waves at different segments of the aperture. The beam tilt angle can typically be controlled by regulating β whereas α distribution over the aperture controls side-lobe-level (SLL). Four segments are marked in **Figure 1(a)** as an illustrative example. In the case of a conventional phased-array antenna, these four segments represent four physical elements, i.e. antennas, where β and α of each can be controlled in straightforward approaches by using phase shifters and attenuators respectively, or with a fully passive custom-built feeding network with proper delay lines and by applying the power-splitting technique. All these elements make the final EM aperture together with an engineered beam as β and α are governed at different positions of the aperture.

Now consider the case where these four elements are located in such a way that they are not able to have a sensible impact on each other to build up a large EM aperture. Under this circumstance, each element acts as an individual aperture as shown in **Figure 1(b)** with its specific radiation properties. This configuration of elements can be applied in multiple input multiple output (MIMO) systems. With a dedicated port for each element, this configuration represents space diversity provided that the cross-correlation between the ports is kept low. It is also possible to use a single element and connect more than one port to it. In this case, each port belongs
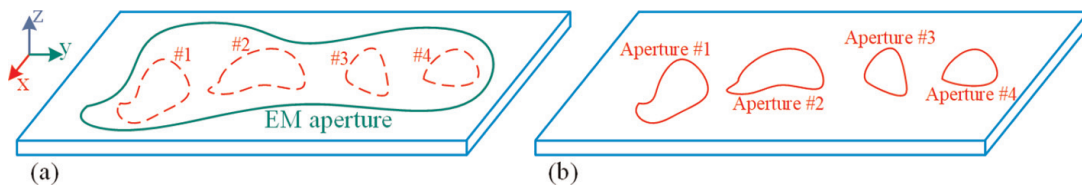
Figure 1.
Aperture formation. (a) The case where four elements make a large aperture altogether and (b) the case where four elements create four separated apertures.

to a specific radiation state or the so-called mode. Having orthogonal modes in this scenario will lead to a low cross-correlation between the ports, making the structure a good candidate for MIMO systems. This orthogonality can be obtained in radiation patterns (pattern diversity) or polarization (polarization diversity) or a combination of both.

Let us move back to the large EM-aperture of **Figure 1(a)**. The envision of such a large aperture is not limited to just phased-array antennas and can be obtained by several means including but not limited to leaky-wave structures, reflectarrays, and transmitarrays. Forming the beam in such structures is also fulfilled by regulating β and α over the aperture but in approaches different from conventional phased arrays. One approach is to employ the holography technique [1] to govern β on the structure and to correspondingly control the tilt angle of beam(s) which is known as "holographic beamforming".

This chapter presents the principles of the holography technique and then explores its capability to form the beam. To this end, some background information on leaky-wave structures and reflectarrays is required.

2. Holographic-based antennas

2.1 Holographic-based leaky-wave antennas

Let us start with the application of holography in leaky-wave antennas. A holographic leaky-wave antenna is a type of antenna that utilizes the principles of holography and leaky-wave propagation to construct the beam and achieve beam scanning capabilities [2]. A leaky-wave antenna (LWA) operates by "leaking" EM energy along its length, which leads to the formation of a propagating wave [3]. Unlike conventional resonating antennas that typically radiate energy perpendicular to the antenna's length, LWAs emit energy at an angle θ_m along their length. This tilt angle can be controlled by regulating the phase constant β of the guided waves across the structure and formulated as [4]:

$$\theta_m \approx \sin^{-1}\left(\frac{\beta}{k_0}\right), \tag{1}$$

where k_0 being the free-space wavenumber. Considering (1), θ_m will have a real answer if and only if $|\beta| < k_0$. This means that LWAs support fast waves on the guide.

Holography, which originates from optics, is a technique to achieve a desired β on the structure by governing the phase distribution on the structure. As β is controlled in an LWA, the tilt angle of the constructed beam can be specified by (1). This technique is summarized below:

Having a dielectric slab on the *xy* plane to design the aperture on, the first step is to define two field distributions on the structure known as reference wave E_{ref} and object wave E_{obj}, generated by two hypothetical sources. To be more explicit, a source should be defined somewhere within the slab where it is aimed to place an actual surface-wave launcher (SWL). For a lossless structure, an ideal hypothetical source located at $(x = 0, y = 0)$ will generate a radially expanded field distribution on the slab for both TM and TE surface waves which can be formulated as below [5]:

$$E_{\text{ref}} = A e^{-j\beta_r r}, \tag{2}$$

where $r = \sqrt{x^2 + y^2}$ and A is the wave amplitude. This is schematically shown in **Figure 2(a)**. It is clear that the location and type of this source can be in a variety of forms. For example, it is possible to place a number of ports at one end of the slab to generate parallel phase lines as shown in **Figure 2(b)** with the formulated reference wave of $E_{\text{ref}} = A e^{j\beta_y y}$. It is also possible to locate the source somewhere out of the slab as presented in **Figure 2(c)**. Under this circumstance, the final structure will not recognize as an LWA; this case is explained more in the next section.

The next step is to define an object wave E_{obj} on the slab. To this end, another hypothetical source should be defined far from the slab toward the direction of the desired constructed beam. The slab is illuminated by this source and the corresponding induced waves should be calculated which represents E_{obj}. For example, for a beam desired to be formed toward (θ_m, ϕ_m), the induced E_{obj} is obtained by the mapping as below:

$$E_{\text{obj}} = B e^{jk_0 \{ \sin(\theta_m) \cos(\phi_m) x + \sin(\theta_m) \sin(\phi_m) y \}}, \tag{3}$$

where B is the amplitude of the object waves.

The next step is to calculate the superposition of $E_s = E_{\text{ref}} \times E_{\text{obj}}$ as an interference pattern where $\angle E_s$ defines the desired EM hologram.

The aforementioned steps of calculating E_{ref}, E_{obj}, and E_s make the "recording" process altogether which means to record the impact of the influencing parameters on the slab. For example, consider a case where an ideal source generates E_{ref} as presented in **Figure 3(a)** on the slab at a specific frequency. With a defined object wave toward $(\theta_m = \pi/4, \phi_m = 2\pi/3)$, the obtained E_{obj} on the slab is shown in
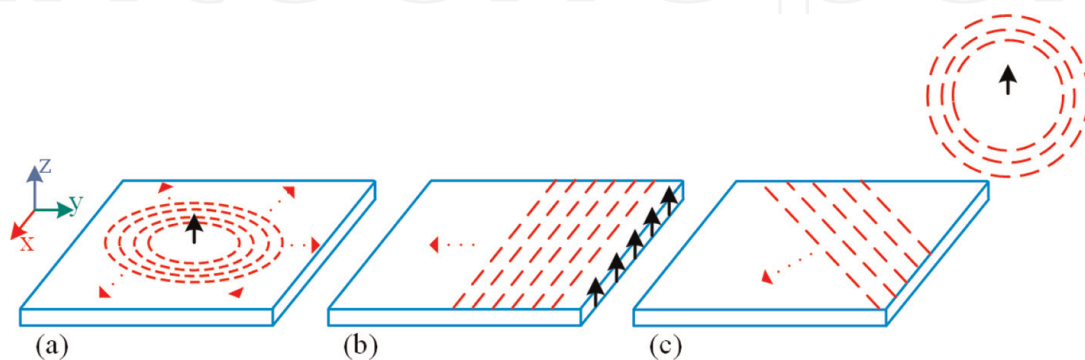

(a) (b) (c)

Figure 2.
Different forms of reference wave on the slab. (a) Radial reference wave by an ideal single source at the center of the slab, (b) parallel reference wave formed by a number of sources at one edge of the slab and (c) induced reference wave from a source located outside the slab.
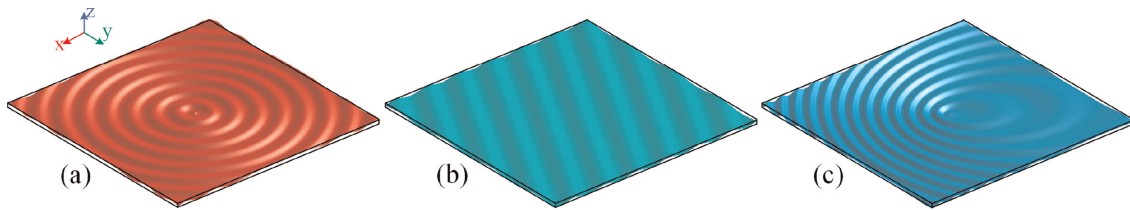
Figure 3.
Recording process: (a) E_{ref} with an ideal source at the center of the slab, (b) E_{obj} in case of $(\theta_m = \pi/4, \phi_m = 2\pi/3)$, and (c) the obtained EM hologram.
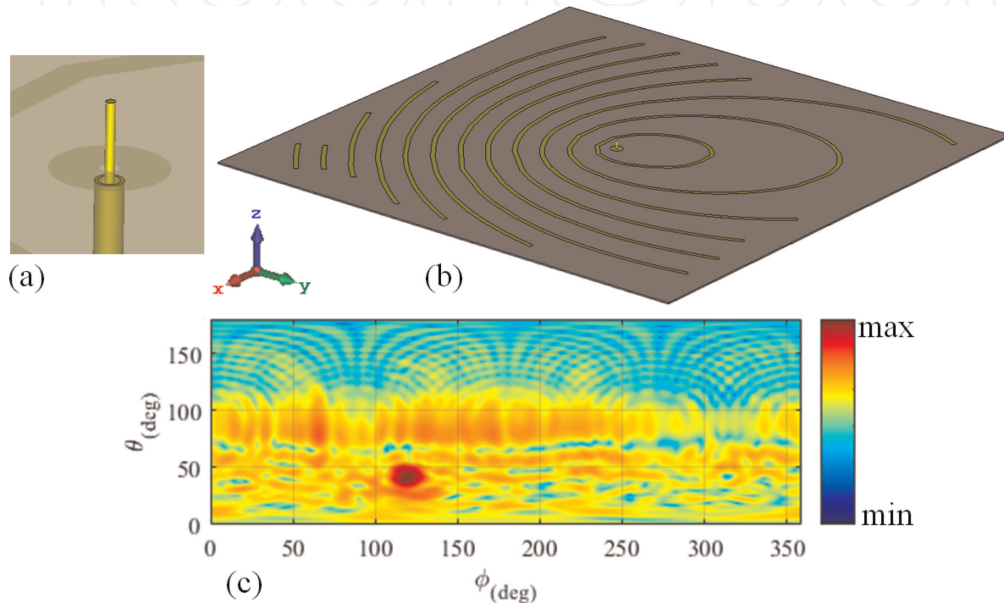

Figure 4.
Reconstruction process: applying (a) surface-wave launcher, and (b) metal strips on the slab. (c) The constructed normalized radiation pattern.

Figure 3(b) for the corresponding k_0. In this case, the pattern of the EM hologram is derived as presented in **Figure 3(c)**.

To embody a real-world structure from the calculated EM hologram, it is required to apply an SWL, exactly at the location where the hypothetical source has been placed in the recording process to be able to generate a field distribution as much similar to the derived E_{ref} as possible. Then, a quasi-periodic pattern of scatterers, with the geometry and lattice inspired by $\angle E_s$ must be applied on the slab to locally sample the generated field distribution of the SWL. The scatterers can be printed metal-strips, sub-wavelength patches of arbitrary shape, dielectric cubes, or any other component that can scatter the launched surface waves on the slab. The process of applying the appropriate SWL and pattern of scatterers on the slab is called "reconstruction".

When the structure in hand is excited by its SWL, the induced surface waves will be leaked out to the open environment toward the predefined tilt angle of (θ_m, ϕ_m) which makes a holographic-based LWA (HLWA).

As an example, an open-ended coaxial cable presented in **Figure 4(a)** can be applied on a grounded dielectric slab to generate TM surface wave distribution similar to **Figure 3(a)**. The surface-wave sampling can be performed by printing metal strips on the local maxima of the calculated EM hologram in **Figure 3(c)** which is presented in **Figure 4(b)**. When this structure is excited, the simulated normalized radiation pattern is obtained as presented in **Figure 4(c)**. This shows that the constructed beam

is pointed well to the predefined angle of interest at the very first steps of the design which is $(\theta_m = \pi/4, \phi_m = 2\pi/3)$.

2.2 Holographic-based reflectors

As briefly pointed out in **Figure 2(c)**, the holography technique can be expanded to the case where the initial source is located outside the slab's body. In this case, the obtained structure will be a holographic-based reflector (HR) [6].

This time, let us sample the EM hologram by using a number of printed sub-wavelength squared-shape patches. These patches will form a quasi-periodic structure where their size is modulated based on the holography technique. In periodic structures, the smallest geometry that is repeated in a fashion is called a unit cell. In this case, the unit cell is a small portion of the dielectric slab with a single printed patch on one side and a full ground plane on the other side as shown in **Figure 5(a)**. The analysis of structure requires characterizing the surface impedance $Z_{\text{surf}} = E_t/H_t$ with E_t and H_t representing the tangential electric and magnetic fields respectively. The obtained structure is then an artificial impedance surface, commonly referred to as a metasurface.

The recording process in Section 2.1 is needed to be modified at the outset to reflect the location of the initial source, i.e. the feeder, on (2).

With an ideal feed located at $\left(x_f, y_f, z_f\right)$ and the slab on the xy plane in a standard right-handed coordinate system, E_{ref} is modified as

$$E_{\text{ref}} = Ae^{-jk_0r}, \tag{4}$$

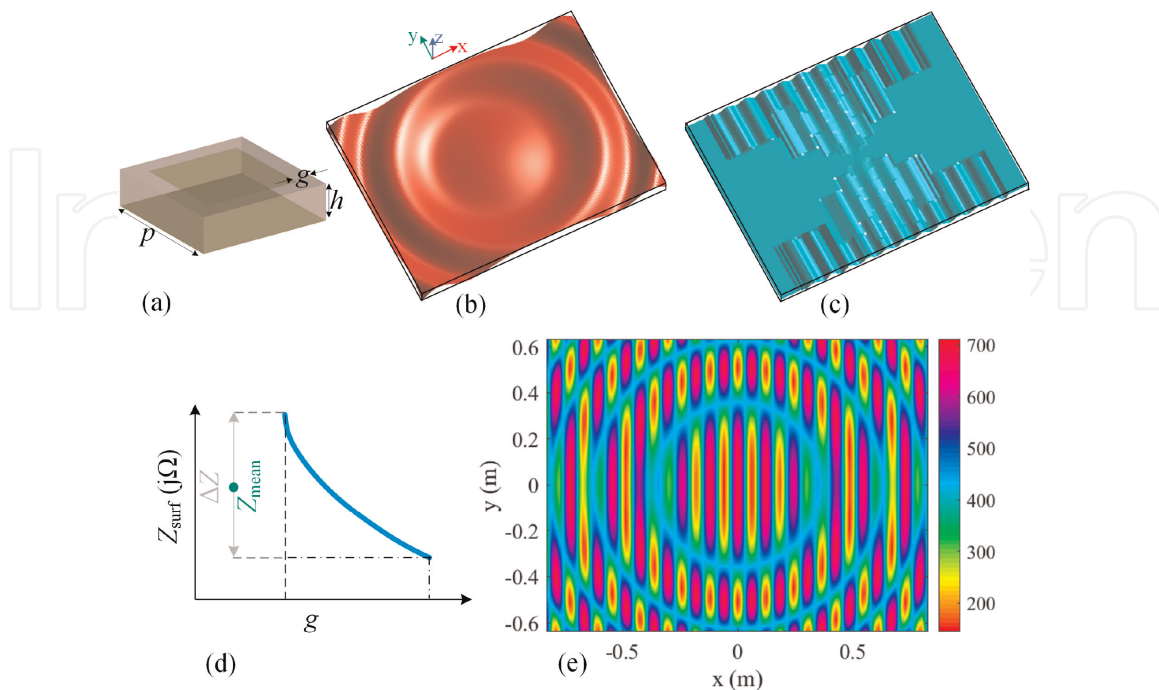where $r = \sqrt{\left(x - x_f\right)^2 + \left(y - y_f\right)^2 + z_f^2}$.

Figure 5.
(a) The applied unit cell, a schema of (b) E_{ref} and (c) $E_{obj}^{\kappa=1} + E_{obj}^{\kappa=2}$, (d) Z_{surf} versus patch size variation and (e) the obtained $Z(x,y)$ on the surface [7].

Figure 5(b) shows the obtained E_{ref} when the feeder is placed at $\left(x_f, y_f, z_f\right) =$ (0,0,2.5m) for a 1.65 m $\times$ 1.25 m large dielectric sheet at $f = 3.5$ GHz [7].

In the holography technique, it is possible to define more than one main beam for the final constructed radiation pattern. Under this circumstance, a summation of the respective object waves will define the final distribution of E_{obj} on the slab. Each object wave is derived by (3) toward the angle of interest. It is aimed in this structure to obtain two reflected beams to $(\theta_{\kappa=1}, \phi_{\kappa=1}) = (45°, 0)$ and $(\theta_{\kappa=2}, \phi_{\kappa=2}) = (-45°, 0)$. The calculated $E_{obj} = E_{obj}^{\kappa=1} + E_{obj}^{\kappa=2}$ is presented in **Figure 5(c)**.

In order to derive the EM hologram, it is now required to conduct a study on Z_{surf} regarding the unit cell of the structure. This can be calculated by sweeping the phase delay (ϕ_D) across the unit cell with periodicity of p as follows [8]:

$$Z_{surf} = jZ_0 \sqrt{\left(\frac{\phi_D}{k_0 p}\right)^2 - 1}, \tag{5}$$

where Z_0 is the free-space impedance. This can be fulfilled by using the eigenmode solver of a full-wave simulator for a specific size of the square patch. Then, the size of the patch must be varied and the calculation repeated to determine the span range of surface impedance ΔZ with the mean value Z_{mean} over the range of patch size variation. This is schematically shown in **Figure 5(d)**.

Having all the above-mentioned information, it is possible to define the EM hologram pattern based on the impedance distribution as below [1]:

$$Z(x, y) = j\left(Z_{mean} + \frac{\Delta Z}{2m} \mathrm{Re}\left[\left(\sum_{\kappa=1}^{m} E_{obj}^{\kappa}\right) E_{ref}^*\right]\right), \tag{6}$$

where m is the number of beams which equals 2 in this case study.

It is shown that $Z_{mean} = 428.16\,j\Omega$ and $\Delta Z = 566.51\,j\Omega$ for the studied range of patch-size variation [7]. This results in an impedance distribution of **Figure 5(e)** as the EM hologram.

The reconstruction process is to use **Figure 5(d)** and **(e)** to modulate the size of patches on each unit cell and print them on the slab. This will lead to a structure shown in **Figure 6(a)**. When this metasurface reflector is illuminated by a feed horn
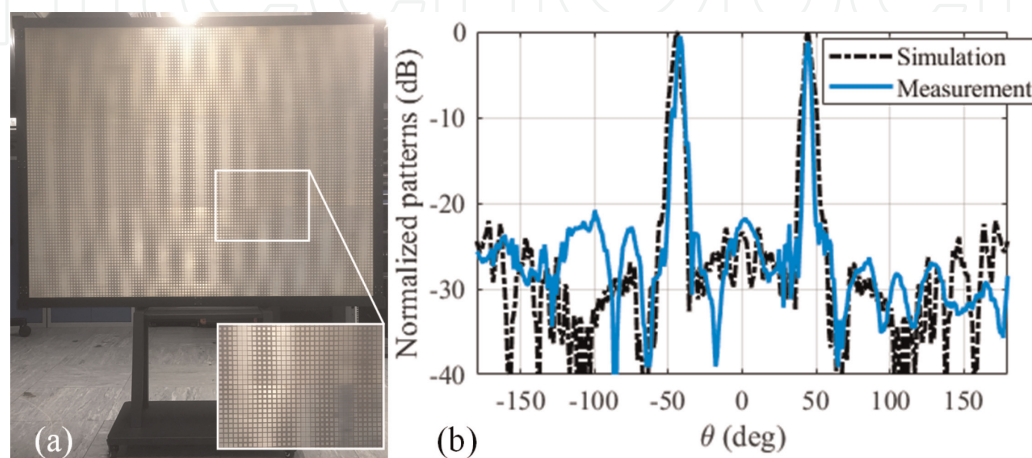

Figure 6.
(a) The metasurface reflector and (b) simulated and measured normalized radiation patterns [7].

located at the position defined during the recording process, the reflected beams from the surface are formed as presented in **Figure 6(b)** which is in line with the defined object waves.

3. Reconfigurable intelligent surface (RIS)

Another possible scenario is the case when the initial source is located outside the surface, but far from the structure. Assume an ideal initial source located at the angle of $(\theta_s = \pi/6, \phi_s = \pi/4)$ with respect to the surface normal far from the structure. Following the routine explains in Section 2.1 and 2.2, E_{ref}, E_{obj}, and the EM hologram patterns are calculated as shown in **Figure 7(a)**, **(b)**, and **(c)** respectively provided that the reflected beam is aimed to be pointed to $(\theta_m = \pi/3, \phi_m = \pi/6)$.

To translate this mechanism into a practical format, this is the case when the surface reflects the incoming waves from a far-located source to a desired direction. This is not a simple mirror reflection where there is no control over the angle of reflection; indeed, the reflection angle can be engineered in this case using the holography technique. This brings a new idea for the future generation of cellular networks.

Consider a case where there is a blind spot within the area under the coverage of a base station (BS). The conventional approach to providing coverage for this blind spot is to add a new BS in the network. However, this method can be expensive and sometimes very challenging regarding the environmental barriers in an area. The idea is to locate a surface in the line of sight (LoS) of the BS so that it can be illuminated by the BS. Then the receiving EM waves reflect back to that blind spot to recycle the waves and provide coverage without adding a new BS. It is possible to reconfigure the response of the surface by applying some components like Varactor or PIN diodes on each unit cell and recalculating the EM hologram for each state of reflection. Under this circumstance, the obtained structure is called a reconfigurable intelligent surface (RIS) [9]. This scenario is schematically shown in **Figure 8(a)**.

Note that holography is not the only technique to regulate the response of the RIS. The generalized Snell's law of reflection (GSR) can also be used in this regard [10]; a GSR-based RIS prototype [11] is shown in **Figure 8(b)**.

One of the biggest problems for RIS to be industrialized and practically applied in real-world networks is its very low aperture efficiency (η_a). This will be more challenging for the uplink scenario when the user attempt to connect BS via RIS. To have a more clear idea about this problem, consider a rectangular reflecting surface with a planar dimension of $X \times Y$, illuminated by a feed horn, distanced by R as presented in **Figure 9(a)**. The feeder's radiation pattern can be expressed by $\cos^{q_E}(\theta)$ and $\cos^{q_H}(\theta)$
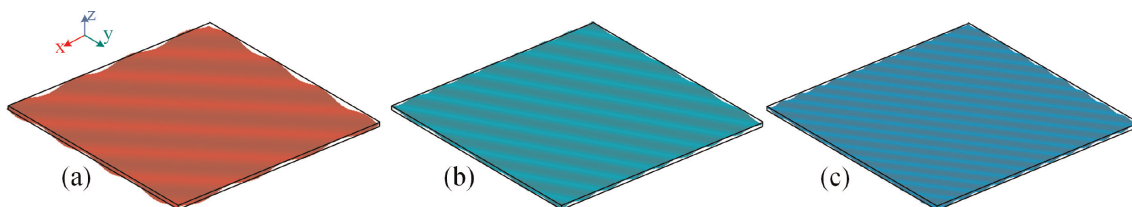

Figure 7.
Recording process: (a) E_{ref} with an ideal source at the angle of $(\theta_s = \pi/6, \phi_s = \pi/4)$ with respect to the surface normal located far from the structure, (b) E_{obj} in case the reflected beam is aimed to be pointed to $(\theta_m = \pi/3, \phi_m = \pi/6)$, and (c) the obtained EM hologram.
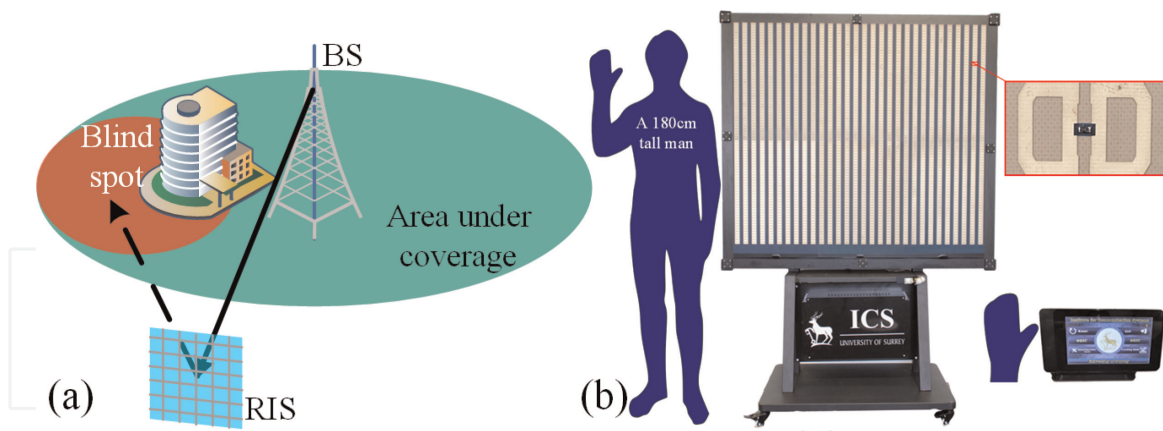
Figure 8.
(a) The coverage provisioning via reconfigurable intelligent surface (RIS) for a blind spot and (b) a prototype example of RIS [11].
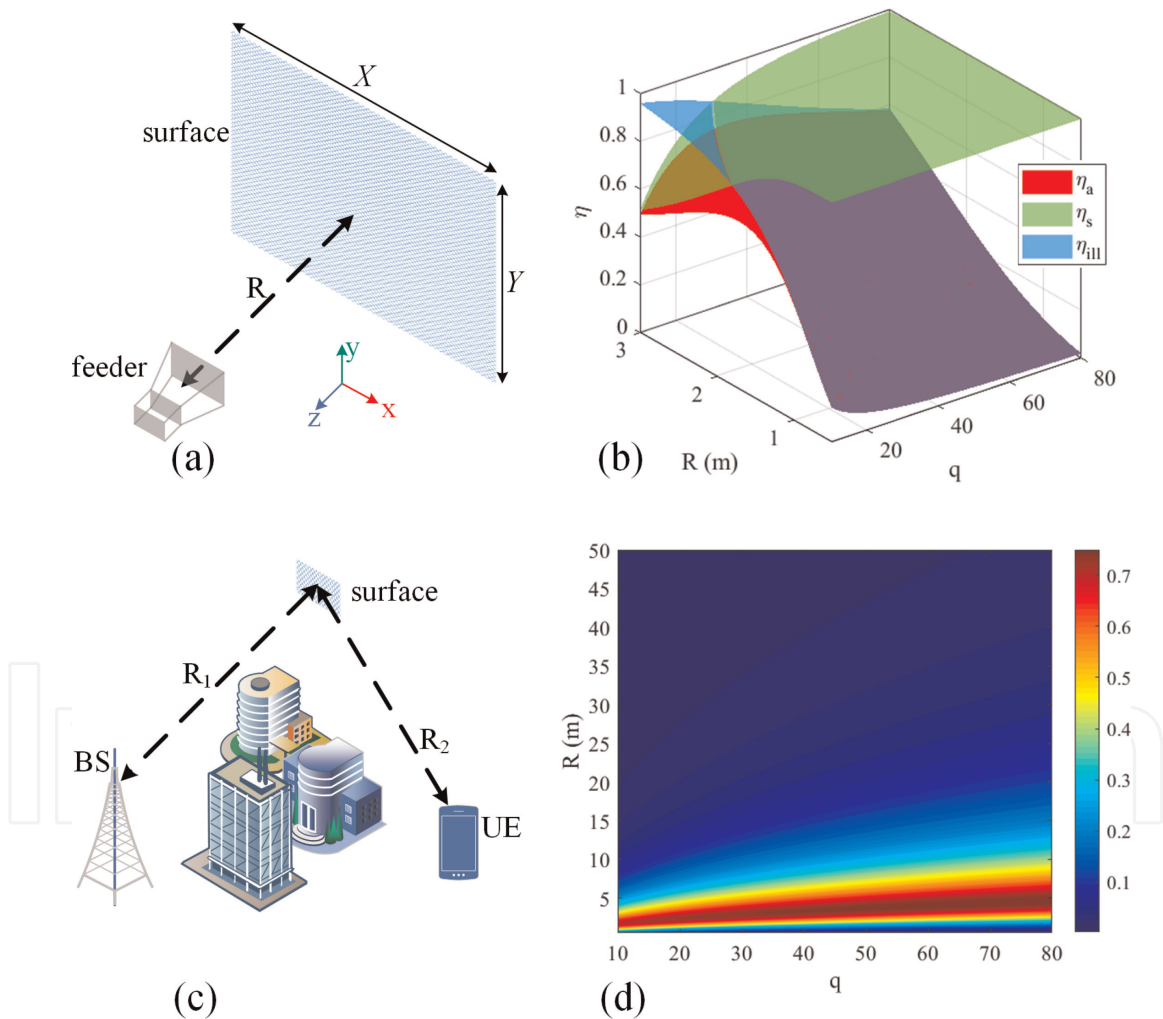

Figure 9.
(a) The overall geometry of a reflective surface illuminated by a feeder, (b) the theoretical aperture efficiency when the feeder is not far from the aperture, (c) a schema of using reflective surfaces to provide the coverage for the user in the blind spot region of the BS, and (d) the theoretical aperture efficiency when the feeder is located relatively far from the aperture.

at the E-plane and H-plane respectively. Product of the illumination (η_{ill}) and spillover (η_s) efficiencies is then defines η_a. In case of rectangular surfaces, η_{ill} can be calculated by [12]:

$$\eta_{ill} = \frac{I^2}{sII}. \tag{7}$$

where $s = X \times Y$ and

$$I = \int_{x=-X/2}^{X/2} \int_{y=-Y/2}^{Y/2} \left\{ \frac{1}{\sqrt{R^2 + x^2 + y^2}} \left[\left(\frac{R}{\sqrt{R^2 + x^2 + y^2}} \right)^{q_E+2} \frac{y^2}{x^2 + y^2} \right. \right.$$
$$\left. \left. + \left(\frac{R}{\sqrt{R^2 + x^2 + y^2}} \right)^{q_H+1} \frac{x^2}{x^2 + y^2} \right] \right\} dydx, \tag{8}$$

with

$$II = \int_{x=-X/2}^{X/2} \int_{y=-Y/2}^{Y/2} \left[\left(\frac{R}{\sqrt{R^2 + x^2 + y^2}} \right)^{2q_E} \frac{y^2}{x^2 + y^2} \right.$$
$$\left. + \left(\frac{R}{\sqrt{R^2 + x^2 + y^2}} \right)^{2q_E} \frac{x^2}{x^2 + y^2} \right] \frac{R}{\left(\sqrt{R^2 + x^2 + y^2} \right)^3} dydx. \tag{9}$$

Under this circumstance, η_s reads:

$$\eta_s = \frac{II}{III}, \tag{10}$$

with

$$III = \pi \left(\frac{1}{1 + 2q_E} + \frac{1}{1 + 2q_H} \right). \tag{11}$$

Now consider the rectangular aperture of **Figure 6**(a). Recall that the physical size of the aperture is $s = 1.65$ m $\times 1.25$ m at 3.5 GHz. With a symetrical radiation pattern at the feeder, $q = q_E = q_H$ and η_{ill} and η_s are obtained by (7) and (10) respectively, followed by calculation of $\eta_a = \eta_{ill} \times \eta_s$. The result is shown in **Figure 9(b)** for different values of $q = 10 \sim 80$ and $R = 0.5 \sim 3$ m. This shows that it is possible to realize optimum values of q and R to use a specific feed horn and locate it at a specific distance from the surface to obtain the maximum possible η_a. This is a routine step of designing reflectarray antennas and metasurface reflectors. However, in the case of RIS where there is no control on q and R, it is not possible to customize the structure to reach the optimum η_a.

Figure 9(c) shows a schema of applying the surface of **Figure 6(a)** for coverage provisioning purposes. Note that this surface has a very large size comparing to the operating wavelength which can potentially be a positive factor for η_a. We repeat the same calculation, but this time the distance range is expanded to $R = 0.5 \sim 50$ m. The result is shown in **Figure 9(d)**. As it is clear, a massive region of this plot shows a very low η_a which can make the structure impractical for real-world applications. This will be more challenging when we pay attention to two factors, 1st: in cellular networks,

the cell radius is much longer than 50 m, this means that the situation is even worse than **Figure 9(d)**; 2nd: for the uplink connection, the user equipment (UE) will have a very low gain (or low q) which will make the connection very challenging if not impossible (see **Figure 9(d)** for low values of q and high R). Finally, it should be noted that these are all theoretical calculations; when it comes to practice, the obtained η_a is expected to be relatively lower than the theory. This is also true even for reflectarray antennas where the feeder is optimized.

4. Comparison between holographic, MIMO, and phased-array beamforming

Consider a case when printed patches are used in three different structures, i.e. a holographic-based metasurface, a phased-array antenna, and a MIMO system. The only common thing between these three is the repeating geometry of patches across the structure. The detailed functionality of these patches is as below:

- Holographic-based metasurface: in this case, the printed patches are used to sample an induced/launched surface wave on the structure. The size of these patches is in the sub-wavelength scope and varies. This variation in size is known as modulation which is governed based on the holography technique[1]. The obtained structure will be an HLWA or an HR with respect to the location of the initial feeder. It is possible to form more than one beam by applying the superposition technique and tilting each of them to the direction of interest. **Figure 10(a)** schematically shows a multi-beam HR. With respect to **Figure 1**, this structure is a single aperture.

- Phased-array antenna: the size of patches is relatively bigger in the scopes of half-wavelength. Therefore, each patch is a resonating element. The element spacing is more than the case of HR metasurface, but should not be more than a wavelength or half a wavelength to stop forming unwanted grating lobes. Each element has typically a port where the corresponding amplitude and phase can be controlled to not only control the tilt angle but also to regulate the obtained SLL. A 4-element planar phased-array antenna with a tilted beam is schematically shown in **Figure 10(b)**. Regarding **Figure 1**, these elements form a single aperture altogether.
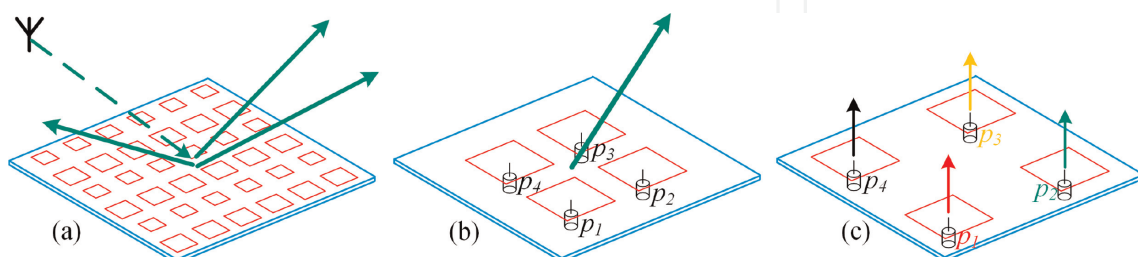

Figure 10.
(a) A multibeam metasurface reflector, (b) a tilted-beam phased-array antenna and (c) a 4-element MIMO system.

---

[1] Note that this is not just limited to the holography, other methods like GSR can also be used.

- MIMO system: the size of patches is again in the scopes of half-wavelength to make a resonating element. However, the spacing between elements is managed to decrease the coupling between elements. When there is a port for each element, this low mutual coupling can decrease the cross-correlation between the ports which can be a good candidate to be used in MIMO systems. As each element is functionally separated from the others, it is common to be called an embedded element. In this case, each embedded element has its own radiation characteristics. A schema of a 4-element MIMO system is presented in **Figure 10(c)**. This structure has four separate apertures considering **Figure 1**.

5. Conclusions

The holography technique and its application in forming the beam in electromagnetic structures are explained in this chapter. Leaky-wave antennas, metasurface reflectors, and reconfigurable intelligent surfaces (RISs) are assessed in this regard. The aperture efficiency of RIS is also studied which is one of the main barriers to industrializing this component in future cellular networks. A comparison is made between the functionality of the smallest building blocks in holographic-base metasurfaces, phased array antennas, and MIMO systems.

Conflict of interest

The authors declare no conflict of interest.

Author details

Ali Araghi[1]* and Mohsen Khalily[2]

1 University College London (UCL), London, United Kingdom

2 University of Surrey, Guildford, United Kingdom

*Address all correspondence to: a.araghi@ucl.ac.uk

IntechOpen

References

[1] Fong BH, Colburn JS, Ottusch JJ, Visher JL, Sievenpiper DF. Scalar and tensor holographic artificial impedance surfaces. IEEE Transactions on Antennas and Propagation. 2010;**58**(10): 3212-3221

[2] Araghi A, Khalily M, Xiao P, Tafazolli R. Holographic-based leaky-wave structures: Transformation of guided waves to leaky waves. IEEE Microwave Magazine. 2021;**22**(6):49-63

[3] Jackson DR, Caloz C, Itoh T. Leaky-wave antennas. Proceedings of the IEEE. 2012;**100**(7):2194-2206

[4] Xu F, Wu K. Understanding leaky-wave structures: A special form of guided-wave structure. IEEE Microwave Magazine. 2013;**14**(5):87-96

[5] Rusch C, Schäfer J, Gulan H, Pahl P, Zwick T. Holographic mmW-antennas with TE$_0$ and TM$_0$ surface wave launchers for frequency-scanning FMCW-radars. IEEE Transactions on Antennas and Propagation. 2015;**63**(4): 1603-1613

[6] Karimipour M, Komjani N. Holographic-inspired multibeam reflectarray with linear polarization. IEEE Transactions on Antennas and Propagation. 2018;**66**(6):2870-2882

[7] Araghi A, Khalily M, Xiao P, Wang F, Tafazolli R. Systematic design of a holographic-based metasurface reflector in the sub-6 GHz band. IEEE Antennas and Wireless Propagation Letters. 2022; **21**(10):1960-1964

[8] Patel AM, Grbic A. A printed leaky-wave antenna based on a sinusoidally-modulated reactance surface. IEEE Transactions on Antennas and Propagation. 2011;**59**(6):2087-2096

[9] Khalily M, Yurduseven O, Cui TJ, Hao Y, Eleftheriades GV. Engineered electromagnetic metasurfaces in wireless communications: Applications, research frontiers and future directions. IEEE Communications Magazine. 2022; **60**(10):88-94

[10] Díaz-Rubio A, Asadchy VS, Elsakka A, Tretyakov SA. From the generalized reflection law to the realization of perfect anomalous reflectors. Science Advances. 2017;**3**(8): e1602714

[11] Araghi A, Khalily M, Safaei M, Bagheri A, Singh V, Wang F, et al. Reconfigurable intelligent surface (RIS) in the sub-6 GHz band: Design, implementation, and real-world demonstration. IEEE Access. 2022;**10**: 2646-2655

[12] Zebrowski M. Illumination and spillover efficiency calculations for rectangular reflectarray antennas. High Frequency Design. 2012;**1**:28-38